Free-fermion descriptions of parafermion chains and string-net models

Konstantinos Meichanetzidis, Christopher J. Turner, Ashk Farjami, Zlatko Papić, and Jiannis K. Pachos
School of Physics and Astronomy, University of Leeds, Leeds LS2 9JT, United Kingdom

(Received 9 June 2017; revised manuscript received 3 January 2018; published 2 March 2018)

Topological phases of matter remain a focus of interest due to their unique properties: fractionalization, ground-state degeneracy, and exotic excitations. While some of these properties can occur in systems of free fermions, their emergence is generally associated with interactions between particles. Here, we quantify the role of interactions in general classes of topological states of matter in one and two spatial dimensions, including parafermion chains and string-net models. Surprisingly, we find that certain topological states can be exactly described by free fermions, while others saturate the maximum possible distance from their optimal free-fermion description [C. J. Turner *et al.*, Nat. Commun. **8**, 14926 (2017)]. Our work opens the door to understanding the complexity of topological models by establishing new types of fermionization procedures to describe their low-energy physics, thus making them amenable to experimental realizations.

DOI: 10.1103/PhysRevB.97.125104

I. INTRODUCTION

A striking feature of many-body systems is their ability to exhibit collective phenomena without analog in their constituent particles. Many recent investigations into exotic statistical behaviors focus on topologically ordered systems [1] that support anyons [2,3]. These systems, such as spin liquids [4] and fractional quantum Hall states [5], exemplify the nonperturbative effects of interactions in many-electron systems. On the other hand, there are systems such as two-dimensional (2D) topological superconductors, which support topological excitations: Majorana zero modes [6,7]. These systems can be modeled by free fermions but lack topological order. Hence, a general question arises: Is it possible (and with what accuracy) to describe a given topological state that supports anyonic quasiparticles, by a Gaussian state corresponding to some free system?

In this paper, we show that a broad class of topological states admit free-fermion descriptions. We use the interaction distance $D_{\mathcal{F}}$ [8] to measure their distinguishability from free-fermion states. We consider parafermion chains [9], which are symmetry-protected topological phases, as well as two-dimensional string nets [10,11], and Kitaev's honeycomb lattice model [12]. These models include renormalization group (RG) fixed points of general families of topological systems with excitations that exhibit anyonic and parafermionic statistics. Generally, we find a broad distribution of $D_{\mathcal{F}}$ values for the ground states of these models. For example, we show that some families of parafermion models nearly maximize $D_{\mathcal{F}}$, while other families have $D_{\mathcal{F}} = 0$ meaning that their ground states, including their edge zero modes, can be written in terms of free fermions. This generalizes the free-fermion description of the Kitaev chain to parafermion chains that have more complex non-Abelian statistics, thus making them amenable to experimental implementation. We further demonstrate that families of Abelian string-net models have a ground state that can be expressed in terms of free fermions. This is highly counterintuitive as free-fermion models are typically not expected to support anyonic statistics. We support these results, both by analytical arguments at the fixed points of various models and by strong numerical evidence away from the fixed points that demonstrate the universal character of $D_{\mathcal{F}}$ within a topological phase. Thus, we establish $D_{\mathcal{F}}$ as a new measure of the complexity of topological models. Moreover, as $D_{\mathcal{F}}$ is defined for a quantum *state* instead of the full spectrum of a system (like the well-known Bethe ansatz techniques), our results open the way for investigating new types of fermionization procedures for describing the low-energy physics of interacting systems with $D_{\mathcal{F}} = 0$.

We proceed as follows. In Sec. II we revise the definition and interpretation of the interaction distance [8], to be applied to ground states of parafermion chains which are introduced and analyzed in Sec. III. In Sec. IV we extend our discussion to string-net models before concluding in Sec. V. Extensive details and supplementary data are presented in the Appendix.

II. INTERACTION DISTANCE

To quantify how far a given state is from any Gaussian state, we define the interaction distance [8] as $D_{\mathcal{F}}(\rho) = \min_{\sigma\in\mathcal{F}} D(\rho,\sigma)$, i.e., the minimal trace distance $D(\rho,\sigma)$ between the reduced density matrix ρ of a bipartitioned system and the manifold $\mathcal{F}$, which contains all free-fermion reduced density matrices σ. It was proven [8] that $D_{\mathcal{F}}$ can be expressed exclusively in terms of the entanglement spectrum [13] as

$$D_{\mathcal{F}}(\rho) = \frac{1}{2}\min_{\{\epsilon\}}\sum_a |\rho_a - \sigma_a(\epsilon)|, \tag{1}$$

where ρ_a and σ_a are the eigenvalues of ρ and σ, respectively, arranged in decreasing order [8]. For Gaussian states we have $\sigma_a = \exp[-\epsilon_0 - \sum_j \epsilon_j n_j(a)]$, where $\{\epsilon_j\}$ is the set of variational single-particle energies corresponding to free-fermion modes and $n_j(a) \in \{0,1\}$ is the modes' occupation pattern corresponding to the given level a of the entanglement spectrum [13,14]. Intuitively, $D_{\mathcal{F}}$ is dominated by the low-lying part of the entanglement spectrum and it reveals the correlations between the effective quasiparticles emerging from interactions [13]. Hence, $D_{\mathcal{F}}$ is expected to be stable under perturbations that do not cause phase transitions [8]. We next apply this measure to quantify the distance of various topological states of matter from free-fermion states. The evaluation of the interaction distance is a complex optimization problem that we solve with analytical arguments and extensive numerical investigations.

III. PARAFERMION CHAINS

The one-dimensional (1D) Ising model can be mapped to the Majorana chain by means of a Jordan-Wigner transformation [15,16]. Similarly, $\mathbb{Z}_{N>2}$ generalizations of the Ising model known as the clock Potts model can be expressed in terms of parafermions [17,18]. Parafermion zero modes may be physically realized at interfaces between 2D topological phases [19,20].

A. Model

The chains are described by the Hamiltonian

$$H_{\mathbb{Z}_N} = -e^{i\phi} \sum_j \alpha_{2j}^\dagger \alpha_{2j+1} - f e^{i\theta} \sum_j \alpha_{2j-1}^\dagger \alpha_{2j} + \text{H.c.}, \quad (2)$$

where f is real and ϕ and θ are the chiral phases of the model. The parafermion operators satisfy the generalized commutation relations $\alpha_j \alpha_k = \omega \alpha_k \alpha_j$ for $k > j$, where $\omega = e^{i2\pi/N}$ and $(\alpha_j)^N = 1$. Majorana fermions correspond to $N = 2$. Recently, phase diagrams of such models have been mapped out numerically [21,22]. Here, we focus on the gapped regime away from the critical points or critical phases [23].

B. Interaction distance at the fixed point

We first consider the system at its fixed point $f = 0$ with $\phi = \theta = 0$ and we place the bipartition between regions A and B at a $(2j, 2j+1)$ link. This gives an N-fold degenerate spectrum [9] $\bar{\rho}(N)$, with $\bar{\rho}_a = 1/N$ for all a, where the overline $\bar{\rho}$ denotes the density matrices with flat spectrum. We would like to determine the optimal free state corresponding to such a flat probability spectrum. Let n be the greatest integer such that $2^n \leqslant N$. We surmise that the optimal free-fermion spectrum is of the form

$$\sigma_{\text{ansatz}} \simeq \text{diag}(N^{-1}, \ldots, N^{-1}, p, \ldots, p), \quad (3)$$

where there are 2^n entries for each value N^{-1} and p. Normalization $\text{tr}(\sigma_{\text{ansatz}}) = 1$ fixes $p = 2^{-n} - N^{-1}$. This ansatz is an element of the variational class $\mathcal{F}$, hence, $D(\bar{\rho}, \sigma_{\text{ansatz}})$ forms an upper bound for $D_{\mathcal{F}}(\bar{\rho}(N))$:

$$D_{\mathcal{F}}(\bar{\rho}(N)) \leqslant 3 - \frac{N}{2^n} - \frac{2^{n+1}}{N}. \quad (4)$$

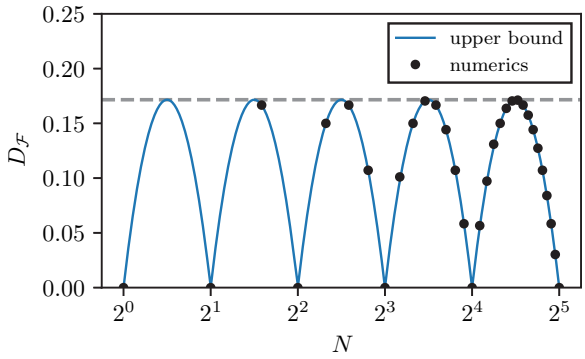

FIG. 1. Interaction distance $D_{\mathcal{F}}(\bar{\rho})$ for flat spectra of rank N. The solid blue line is the analytical upper bound given in (4) and attains maximal value $D_{\mathcal{F}}^{\max}$ (dashed line). The dots are results of the numerical optimization and they coincide with the analytic upper bound.

To evaluate $D(\bar{\rho}, \sigma_{\text{ansatz}})$, we pad the spectrum of $\bar{\rho}(N)$ with zeros, a procedure always viable as it leaves the entropy invariant [8]. We find that the numerically computed $D_{\mathcal{F}}(\bar{\rho}(N))$ is in remarkable agreement with this upper bound, as shown in Fig. 1. We analytically proved that the two values coincide for $N \leqslant 6$, while we numerically verified it for up to $N = 2^8$ (see Appendix). Hence, we conjecture that the upper bound of Eq. (4) is the *exact* maximum of $D_{\mathcal{F}}(\bar{\rho})$. This result also applies to the 2D string-net models presented below.

From Eq. (4) we find that the maximum of the interaction distance is $D_{\mathcal{F}}^{\max} = 3 - 2\sqrt{2}$. This maximum is approached by rational approximations $N/2^n$ of $\sqrt{2}$ for increasing n, as shown in Fig. 1. By the exhaustive numerical maximization $\max_\rho D_{\mathcal{F}}(\rho)$ for random ρ, we have not found states with interaction distance larger than $D_{\mathcal{F}}^{\max}$ (see Appendix). Hence, this appears to be the maximum possible value of the interaction distance *for any state*.

The behavior of the interaction distance for the flat spectra of parafermion chains, shown in Fig. 1, exhibits a recurring pattern, indicating that $\bar{\rho}$ has exactly the same interaction distance as $\frac{1}{2}(\bar{\rho} \oplus \bar{\rho})$. This doubling of the spectrum is equivalent to adding a zero fermionic mode to $\bar{\rho}$, which is decoupled from the rest of the modes [24,25], and thus it is not expected to change its interaction distance. We conjecture that for a generic ρ, i.e., with a nonflat spectrum, we still have $D_{\mathcal{F}}(\frac{1}{2}(\rho \oplus \rho)) = D_{\mathcal{F}}(\rho)$, which is supported by systematic numerical evidence (see Appendix).

In conclusion, we find that $\mathbb{Z}_{N \neq 2^n}$ parafermion chains exhibit $D_{\mathcal{F}} \neq 0$, indicating that they are interacting in terms of complex fermions, while the inequality (4) gave $D_{\mathcal{F}} = 0$ for all $\mathbb{Z}_{2^n}$ models. These results have been derived at the fixed point ($f = 0$ and $\phi = \theta = 0$), and now we address their validity away from the fixed point. The entanglement spectrum and, as a consequence, the interaction distance, can distinguish between the universal and nonuniversal properties of gapped systems [8,13].

C. Off-the-fixed-point and excited states

When the parafermion chain is away from its fixed point, it acquires a nonzero correlation length ξ. To identify the

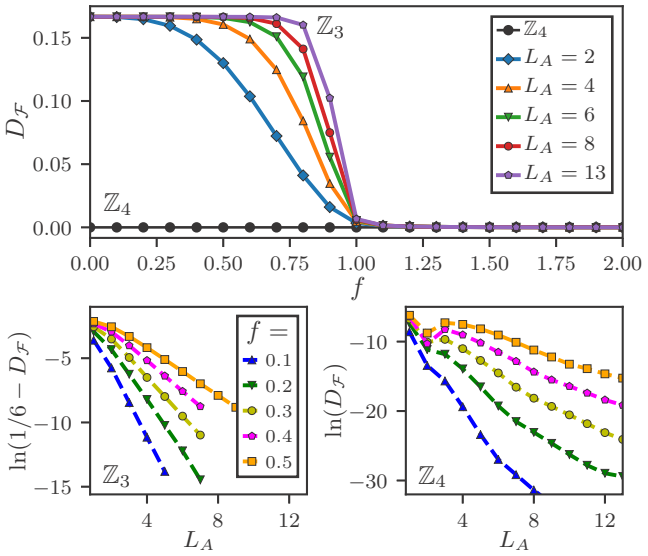

FIG. 2. (Top) Interaction distance for the $\mathbb{Z}_4$ parafermion chain (black line) and $\mathbb{Z}_3$ (all other lines) of length $L = 30$ calculated with DMRG [26,27] for open boundary conditions. The partition size is $L_A = 15$ for $\mathbb{Z}_4$ and for $\mathbb{Z}_3$ we study several L_A indicated in the legend, for a range of f values. With increasing partition size $D_\mathcal{F}$ of $\mathbb{Z}_3$ approaches its fixed-point value producing a step function across the phase transition. (Bottom, left) $\ln(1/6 - D_\mathcal{F})$ for the $\mathbb{Z}_3$ chain ($\phi = \theta = 0$) shows that $D_\mathcal{F}$ converges exponentially to its fixed-point value $D_\mathcal{F}(\bar{\rho}(3))$ as we increase L_A. (Bottom, right) $\ln(D_\mathcal{F})$ for the chiral $\mathbb{Z}_4$ chain ($\phi = \theta = 0.2$) shows that $D_\mathcal{F}$ converges exponentially to its fixed-point value of zero as we increase L_A. Each line in the bottom of the figure is labeled by the value of f.

universal properties of the system through $D_\mathcal{F}$, the linear size L_A of the partition A should be $L_A \gg \xi$. The nonuniversal part is exponentially suppressed in a gapped phase and $D_\mathcal{F}$ predominantly describes the topological properties of the system, as shown in Fig. 2. In this figure, we see that $\mathbb{Z}_4$ has $D_\mathcal{F} = 0$ for any value of f ($\phi = \theta = 0$), while the interaction distance for $\mathbb{Z}_3$ approaches a step function through the phase transition. Figure 2 (bottom, right) shows the exponential convergence to zero of $D_\mathcal{F}$ for $\mathbb{Z}_4$ with $\phi = \theta = 0.2$. Hence, when the parafermion chain is away from criticality, its ground state $D_\mathcal{F}$ is a robust characteristic of the topological phase. The value of $D_\mathcal{F}$ is accurately given by the upper bound (4) for sufficiently large system and partition sizes.

We have also studied the excited states of parafermion models. In the $\mathbb{Z}_{2^n}$ cases, it can be shown that $D_\mathcal{F} = 0$ for all excited states at the fixed point. However, at any finite $f > 0$, the excited states in general have nonzero $D_\mathcal{F}$ (apart from single quasiparticle excitations above the ground state, which remain approximately free for $f > 0$ close to the fixed point). This is consistent with the models being nonintegrable [9] for general f, although its ground state remains Gaussian. There are exceptions to this for special choices of chiral angles, e.g., at $\phi = \pi/2$ and $\theta = \pi$, suggesting that there is a free-fermion description of the $\mathbb{Z}_4$ chain at this point [28].

D. Free parent Hamiltonian

To identify the free-fermion description of the $\mathbb{Z}_4$ ground state, and those of other $N = 2^n$, we employ a matrix product state approach (see Appendix). For simplicity, we consider the $f,\phi,\theta = 0$ fixed point. One can express the ground state of $\mathbb{Z}_{pq}$ in terms of the ground state of $\mathbb{Z}_p \times \mathbb{Z}_q$ (which has the same entanglement spectrum) for any p and q with the help of a unitary rotation. This unitary $\mathcal{U} = \otimes_{j=0}^{L} U$ is a product of single-site unitaries U, acting on each site of the chain (see Appendix), given by

$$U = F^\dagger_{\mathbb{Z}_p \times \mathbb{Z}_q} F_{\mathbb{Z}_{pq}}, \tag{5}$$

where $F_\mathcal{G}$ is the quantum Fourier transform [29] for a finite group $\mathcal{G}$. These can be implemented by simple quantum circuits over qudits forming the prime factorization [30,31] of pq. From this relation between the ground states we can identify the parent Hamiltonian $H_{\mathbb{Z}_{pq}}$, that has the same ground state as $H_{\mathbb{Z}_p \times \mathbb{Z}_q}$:

$$H_{\mathbb{Z}_{pq}} = \mathcal{U}^\dagger H_{\mathbb{Z}_p \times \mathbb{Z}_q} \mathcal{U}, \tag{6}$$

where $H_{\mathbb{Z}_p \times \mathbb{Z}_q}$ is defined similarly to the Hamiltonians in (2). This local Hamiltonian gives rise to the same zero modes localized at the end points of a chain like the $\mathbb{Z}_{pq}$ model, even though their excitation spectra *may not coincide*. In particular, the construction in Eq. (6) explicitly gives the parent free-fermion Hamiltonians $H^{\text{free}}_{(\otimes_n \mathbb{Z}_2)}$ corresponding to all $\mathbb{Z}_{2^n}$ models with $D_\mathcal{F} = 0$.

IV. STRING NETS

We now turn to the string-net models [10,32]. These are 2D RG fixed-point models that support topological order and anyon excitations. The models are defined in terms of irreducible representations or "charges" of a finite group $\mathcal{C} = \{1, \ldots, n\}$, that parametrize the edges of a honeycomb lattice, as shown in Fig. 3 (left). These charges obey the fusion rules $x \times y = \sum_z N^z_{xy} z$, where N^z_{xy} is the multiplicity of each fusion

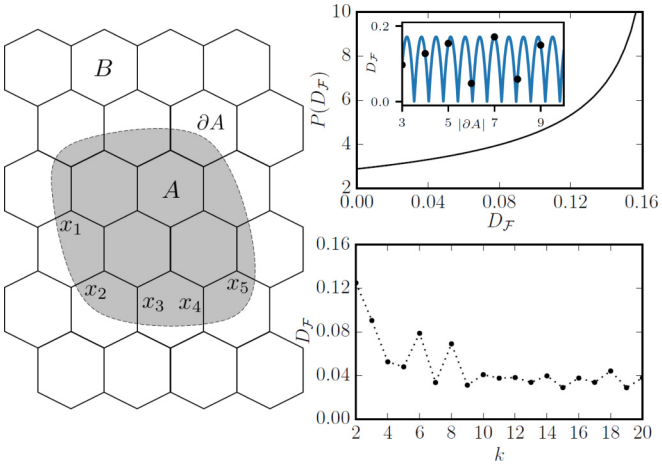

FIG. 3. (Left) The string-net model on a honeycomb lattice with a bipartition into A and B. A configuration of charges x_j is depicted at the links of the boundary ∂A. (Right, top) Distribution $P(D_\mathcal{F})$ of the interaction distance of some $\mathbb{Z}_{N \neq 2^n}$, for varying $|\partial A|$. (Inset) The dots represent the numerically obtained interaction distance for $\mathbb{Z}_3$ as a function of $|\partial A|$. (Right, bottom). Plot of $D_\mathcal{F}$ for $\mathrm{SU}(2)_k$ against k for a partition with $|\partial A| = 3$.

outcome. For each charge x, the quantum dimension d_x is defined that satisfies $d_x \times d_y = \sum_z N_{xy}^z d_z$.

The ground state of a string-net model can be interpreted as a superposition of all configurations of charge loops. The probability spectrum from any bipartition into single-component regions A and B is determined by all string configurations a on the boundary ∂A which fuse to the vacuum

$$\rho_a = \frac{\prod_{j\in a} d_{x_j}}{\mathcal{D}^{2(|\partial A|-1)}}, \tag{7}$$

where $\mathcal{D} = \sqrt{\sum_x d_x^2}$ is the total quantum dimension of the group and x_j is an element of the configuration a of charges at the boundary links, as shown in Fig. 3 (left). Hence, we can directly evaluate the entanglement spectra of all string-net models, Abelian or non-Abelian, and for any partition [33].

A. Abelian models and freedom

We initially consider string nets defined with an Abelian group $\mathbb{Z}_N$. These models have $d_x = 1$ for all $x \in \mathcal{C}$ and thus $\mathcal{D} = \sqrt{N}$. From Eq. (7), we find that the corresponding probability spectrum for any bipartition is flat with degeneracy $N^{|\partial A|-1}$. Hence, the interaction distance $D_\mathcal{F}$ is directly determined from Eq. (4) as in the case of parafermion chains.

Following the mathematical analysis given in the parafermion models, we find that the cases with $N = 2^n$ have $D_\mathcal{F} = 0$ identically, for any partition size. This universal characteristic of these string-net models dictates that their ground states can be described by free fermions. This is a surprising result as anyonic quasiparticles are expected to emerge in interacting systems. Nevertheless, the optimal free states are not necessarily local and their energy spectrum is not necessarily given by filling of single-fermion modes. For $N = 2$ we obtain the well-known toric code [34].

We now show that the fermionization of this model is given in terms of free lattice fermions coupled to a $\mathbb{Z}_2$ gauge field. Kitaev's honeycomb lattice model [12] is an interacting model that supports vortices with Abelian toric code or non-Abelian Ising anyonic statistics, depending on its coupling regime. Nevertheless, for fixed vortex configurations its Hamiltonian is reduced to free fermions living on the vertices of the honeycomb lattice coupled to a static $\mathbb{Z}_2$ gauge field u that resides on its links [12]. When we bipartition the ground state of the system, the reduced density matrix splits into a gauge and a fermionic part [35], i.e., $\rho = \bar{\rho}_u \otimes \rho_\phi$. The gauge part corresponds to a $\mathbb{Z}_2$ flat spectrum giving $D_\mathcal{F}(\bar{\rho}_u) = 0$ and the fermionic part corresponds to free fermions with $D_\mathcal{F}(\rho_\phi) = 0$. This means that ρ, as a tensor product of free-fermion entanglement spectra, has also $D_\mathcal{F}(\rho) = 0$ for any partition, rendering the ground-state Gaussian. Hence, free fermions coupled to a $\mathbb{Z}_2$ gauge field provide the fermionization prescription of the $\mathbb{Z}_2$ string-net model. This is a nontrivial result as the application of the gauge constraint can force the ground state to be non-Gaussian.

For string nets with $N \neq 2^n$, $D_\mathcal{F}$ is always nonzero for any partition. Hence, these states can never be represented by free fermions. In particular, its value depends on the size $|\partial A|$ of the partition signifying that different numbers of anyonic quasiparticles effectively describing the correlations of the ground state can be closer or further away from free-fermion description. We investigate its behavior by studying the distribution $P(D_\mathcal{F})$ of $D_\mathcal{F}$ by varying the size $|\partial A|$ of the boundary for a certain model $\mathbb{Z}_N$. This distribution can be shown to be given by $P(D_\mathcal{F}) = \frac{2}{\ln 2}/\sqrt{1 + D_\mathcal{F}(D_\mathcal{F} - 6)}$, which, surprisingly, is N independent (see Appendix). Hence, there exist partitions that asymptotically maximize $D_\mathcal{F}$ for all $N \neq 2^n$, as shown in Fig. 3 (right, top). Therefore, all $\mathbb{Z}_N$ Abelian string nets either admit a free-fermion description for any partition or they form a class for which the manifestations of interactions are equivalent.

B. Non-Abelian models and nontrivial interaction distance

We next consider the non-Abelian string-net models. For concreteness, we take the finite group to be $\mathrm{SU}(2)_k$ for various levels $k \geqslant 2$. This group gives rise to string-net models that support a large class of non-Abelian anyons, such as the Ising anyons for $k = 2$, with statistics similar to Majorana fermions, or the Fibonacci anyons for $k = 3$, that are universal for quantum computation [36,37]. For simplicity, we consider the interaction distance for a single-site partition that has $|\partial A| = 3$. We find that $D_\mathcal{F} \neq 0$ for all $k \leqslant 20$, as shown in Fig. 3 (right, bottom). Hence, it is not possible to find a free-fermion description of these non-Abelian string-net models. Nevertheless, it is possible to have chiral non-Abelian models that are not RG fixed points, which admit a description of their ground state in terms of free fermions. As we have shown, Kitaev's honeycomb lattice model falls in this category.

V. CONCLUSIONS

We have quantified the effect of interactions in the ground states of broad classes of topological phases of matter in all spatial dimensions. This analysis provides a clear picture of the landscape of RG fixed-point models in terms of their free-fermion representation. As the interaction distance of the fixed-point models appears to be robust against perturbations that do not cause phase transitions, we are able to find universal characteristics of these models. This is in agreement with the interpretation of the interaction distance as the measure of the correlations between the emerging quasiparticles of the system, which are unaffected by its microscopic details. Surprisingly, we discovered that the $\mathbb{Z}_{2^n}$ parafermion chains, as well as $\mathbb{Z}_{2^n}$ string nets, all have ground states with $D_\mathcal{F} = 0$. This is a universal characteristic that holds for any partition of the system and it is stable against perturbations that do not cause a phase transition.

Identifying Gaussianity in the ground state of a model can refine the notion of fermionization procedures employed to solve quantum Hamiltonians. Such procedures are applicable, in the usual sense, if a system has $D_\mathcal{F} = 0$ for all possible bipartitions and in all its eigenstates, while at the same time the energy spectrum is also free. A more subtle possibility appears when $D_\mathcal{F} = 0$ for some eigenstates (and all cuts), but the energy spectrum is not that of free fermions. We believe integrable systems [38] fall into this category. We also note that $D_\mathcal{F} = 0$ for the ground state is in principle compatible with anyon statistics because the latter only emerges when one interpolates adiabatically between different sectors of

the conserved charges of the model [39]. In this sense, our approach generalizes the case of Majorana fermions, to the $\mathbb{Z}_{2^n}$ models that have more complex non-Abelian statistics, but still have a ground state that admits a free-fermion description. This result greatly facilitates their analytical study and opens the way for their experimental realization.

ACKNOWLEDGMENTS

We thank A. Bullivant, P. Fendley, and J. Southall for inspiring comments. This work was supported by the EPSRC Grants No. EP/I038683/1, No. EP/M50807X/1, and No. EP/P009409/1. Statement of compliance with EPSRC policy framework on research data: This publication is theoretical work that does not require supporting research data.

APPENDIX

In this Appendix, we discuss the ansatz and the derived upper bound for flat spectra. We then present numerical evidence that the upper bound is the exact solution for flat spectra. We provide numerical evidence for the zero-mode conjecture $D_{\mathcal{F}}(\frac{1}{2}(\rho \oplus \rho)) = D_{\mathcal{F}}(\rho)$ and the conjecture that the maximum value of the interaction distance is $D_{\mathcal{F}}^{\max} = 3 - 2\sqrt{2}$. Furthermore, we support in detail the statement made in the main text on the existence of an exact mapping of the ground state of the $\mathbb{Z}_4$ chain to that of $\mathbb{Z}_2 \times \mathbb{Z}_2$ using the formalism of matrix product states. Following on, we offer a simple proof for the exactness of the upper bound of $D_{\mathcal{F}}$ for the rank-6 maximally entangled state, inspired by ideas from order theory applied on free-fermion spectra. Next, we calculate the distribution functions of $D_{\mathcal{F}}$ which characterize the parafermion models and string nets. Finally, we calculate $D_{\mathcal{F}}$ for the topologically distinct subregions of a 3D Walker-Wang model.

1. Optimal free ansatz for flat spectra

Here, we describe in detail the construction of the optimal free-fermion description of a flat N-rank entanglement spectrum. We guess that it is optimal to exactly match as many of the highest probability levels as possible. The most that can be matched are 2^n, where n is the greatest integer such that $2^n \leqslant N$. Considering the entanglement energies, i.e., negative logarithms of the eigenvalues of ρ, this is achieved by requiring σ to contain n zero modes. We further assume that the optimal σ has only one further nontrivial mode whose splitting parameter is now fixed by the requirement that the first 2^n levels of σ have eigenvalue N^{-1} leading to the form given in the main text:

$$\sigma \simeq \mathrm{diag}(N^{-1}, \ldots, N^{-1}, p, \ldots, p). \tag{A1}$$

Then, we can write σ as a tensor product of two-level (fermion) modes as

$$\sigma \simeq \bigotimes_i \mathrm{diag}\left(\frac{1}{2} + s_i, \frac{1}{2} - s_i\right), \tag{A2}$$

where for n of the modes $s_i = 0$ and the one remaining mode $s_i = N^{-1}2^n - 1/2$, ensuring that σ is free.

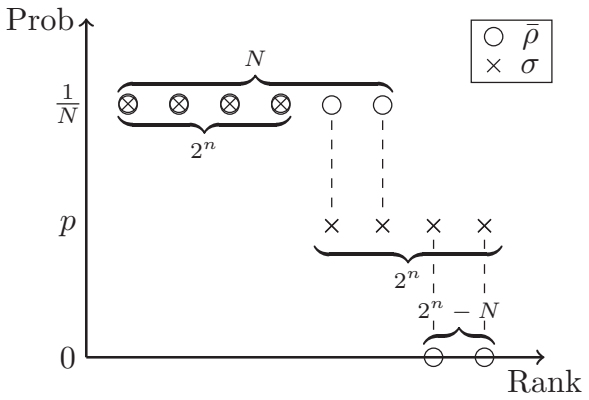

FIG. 4. Probability spectra showing the flat spectrum of degeneracy N (including zeros padding the spectrum to the next power of two) and the corresponding σ_{ansatz} defined in Eq. (A2).

There are two contributions to the upper bound $D(\bar{\rho},\sigma)$. The first is from the entanglement levels with index $2^n + 1 \leqslant k \leqslant N$ for which the probability difference is between N^{-1} and p, illustrated by the dashed lines between the top and middle rows of eigenvalues in Fig. 4. The second is from levels with index $N + 1 \leqslant k \leqslant 2^{n+1}$ for which the probability difference is between 0 and p, illustrated by the dashed lines between the middle and bottom rows of eigenvalues in Fig. 4. In the trivial case where $N = 2^n$ for some n, then $\bar{\rho}(N)$ can be reproduced by n-many zero modes and the spectrum is free with $D_{\mathcal{F}} = 0$ as seen in Fig. 5.

We compared this analytic upper bound with results from numerical optimization for N up to 2^8, where we use the same Monte Carlo basin hopping strategy used successfully previously for the 1D quantum Ising model in a magnetic field [8]. For larger N, the increasing size of the optimization problem results in the numerical minimization failing to consistently find the global minimum. Remarkably, numerical minimization never finds results below the analytic upper bound, making a convincing case that this upper bound is in fact the exact result.

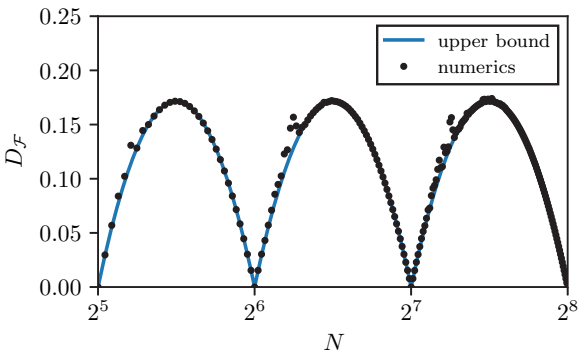

FIG. 5. Interaction distance $D_{\mathcal{F}}(\bar{\rho})$ for flat spectra of rank N. Results of numerical optimization and the analytic upper bound $D_{\mathcal{F}}(\bar{\rho}(N)) \leqslant 3 - \frac{N}{2^n} - \frac{2^{n+1}}{N}$ are compared, revealing that numerical optimization never improves on the analytic upper bound. The numerical data feature deviations above the analytic curve which represent intermittent failure of finding the global minimum.

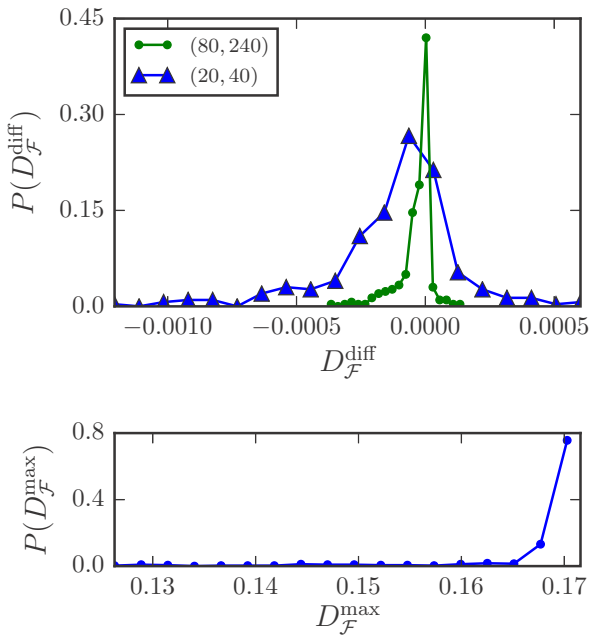

FIG. 6. (Top) Distribution $P(D_{\mathcal{F}})$ of the difference between the interaction distance of random state ρ and its doubly degenerate realization $\frac{1}{2}(\rho \oplus \rho)$. The sample contains 300 instances of ρ. Increasing the number of basins used in the minimizations $D_{\mathcal{F}}(\rho)$ and $D_{\mathcal{F}}(\frac{1}{2}(\rho \oplus \rho))$, respectively, indicated as a tuple (legend), drives the distribution to a sharp peak. (Bottom) Distribution of outputs of the maximization of $D_{\mathcal{F}}$ performed 400 times for spectra of rank randomly selected between 3 and 8. Here, the number of basins in the minimization of $D_{\mathcal{F}}$ is 30. The number of basins for the maximization is randomly selected from the set {5,15,50}. The maximization achieves the conjectured upper bound $3 - 2\sqrt{2} \approx 0.1716$ but never exceeds it.

2. Numerical evidence for conjectures

Here, we provide numerical evidence for conjectures regarding $D_{\mathcal{F}}$ which we state in the main text. In particular, we indicate that the zero-mode conjecture $D_{\mathcal{F}}(\rho) = D_{\mathcal{F}}(\frac{1}{2}(\rho \oplus \rho))$ holds, as well as that the maximal possible value of the interaction distance is $D_{\mathcal{F}}^{\max}$. As stated in Ref. [8], we use a basin-hopping algorithm which collects values of local minima via the Nelder-Mead method for each basin of the cost function landscape. We show that apparent violations of these conjectures correspond to cases where the optimization does not reach a global minimum and increasing the number of basins results in the conjectures holding true.

Let ρ represent a generic diagonal density matrix. Its doubly degenerate version $\frac{1}{2}(\rho \oplus \rho)$ can be interpreted as the result of adding a zero-entanglement energy in the system, where entanglement energy is defined as the negative logarithm of a probability [13]. This becomes clear when considering that each member of a degenerate pair of eigenvalues corresponds to the zero mode being occupied or not. We compute $D_{\mathcal{F}}^{\text{diff}} = D_{\mathcal{F}}(\rho) - D_{\mathcal{F}}(\frac{1}{2}(\rho \oplus \rho))$ for random diagonal density matrices. The distribution $P(D_{\mathcal{F}}^{\text{diff}})$ is peaked at zero, indicating the validity of the zero-mode conjecture, as shown in Fig. 6 (top). The peak is more prominent when the number of basins is increased. Note that $D_{\mathcal{F}}(\frac{1}{2}(\rho \oplus \rho)) \leqslant D(\frac{1}{2}(\rho \oplus \rho), \frac{1}{2}(\sigma \oplus \sigma)) = D_{\mathcal{F}}(\rho)$, where σ is the optimal free state of ρ. The inequality holds because $\frac{1}{2}(\sigma \oplus \sigma) \in \mathcal{F}$ is a member of the variational class $\mathcal{F}$. Thus, we attribute $D_{\mathcal{F}}^{\text{diff}} < 0$ to failure of the minimization in finding the global minimum for $D(\frac{1}{2}(\rho \oplus \rho))$ due to the greater number of input probabilities.

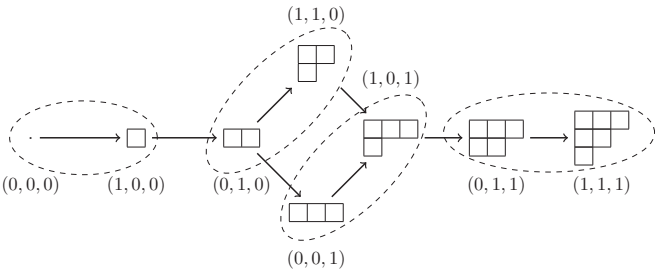

FIG. 7. Hasse diagram for the free-fermion entanglement lattice in the case of three fermionic modes ($\mathcal{F}_3$). Vertices contain the Young diagrams which represent the occupation numbers (n_1,n_2,n_3) of the three modes with which they are labeled. Grouped vertices are renormalized by integrating over the first occupation number to give the vertices of $\mathcal{F}_2$.

Regarding the maximal possible interaction distance, we use yet again basin hopping in order to perform the maximization $\max_\rho D_{\mathcal{F}}(\rho)$. For each instance of ρ, we find $D_{\mathcal{F}}$ by the Nelder-Mead method, with the condition that if the cost function is greater than the conjectured value $3 - 2\sqrt{2}$, then basin hopping is performed for a large enough number of basins so that finding the global minimum is better approximated, which we never find to be above $3 - 2\sqrt{2}$ as shown in Fig. 6 (bottom).

3. Entanglement lattices

Here, we present a view of the structure of free-fermion spectra in terms of order theory, which aids in deriving exact results for $D_{\mathcal{F}}$ in special cases of flat spectra. Each level of a free entanglement spectrum σ is labeled by a set of occupation numbers. We can define a partial order $a \preceq b$ for occupation-pattern labels a and b to hold if and only if $\sigma_a \geqslant \sigma_b$ for any free entanglement spectrum σ. This partial order induces an equivalent covering relation $a \to c$ if and only if for any σ we have $\sigma_a \geqslant \sigma_c$ and there exists no other pattern b such that $\sigma_a \geqslant \sigma_b \geqslant \sigma_b$. In Fig. 7 the vertices are the occupation patterns and the arrows connecting them are the covering relations, forming an example of a Hasse diagram [40]. The example in Fig. 7 is the free entanglement partial order $\mathcal{F}_3$ for the case of three modes.

The partial ordering of the occupation-pattern coordinates is the strongest ordering compatible with any spectrum σ which assigns to each mode k an energy E_k which is nondecreasing in k. This ordering is known as the dominance order [41]. Another way of describing each level is to instead count the occupation of each energy gap. Occupying an energy mode is equivalent to occupying all the energy gaps beneath it, and the transformation between the two pictures is known as majorization. Each energy gap is non-negative but otherwise unconstrained, thus, the strongest partial order compatible with all σ follows a coordinate order in these majorized coordinates. Majorization theory is a familiar topic in quantum information

and has been the source of many fruitful applications (see Refs. [42,43] for example).

Each set of majorized coordinates can be related to a Young diagram where the number of boxes in each column is the corresponding majorized coordinate and the number of boxes in each row labels the energy level occupied by each excitation (see Fig. 7). Choosing a covering relation to mean the addition of a single box to the Young diagram defines a lattice known as Young's lattice, a sublattice of which can be identified as the free entanglement lattice. If we were considering free boson models instead of free fermions, there would be no exclusion of multiple occupancy and the entanglement lattice would be isomorphic to Young's lattice.

Theorem 1. $D_{\mathcal{F}}(\bar{\rho}(2^{n+1}-2)) = D_{\mathcal{F}}(\bar{\rho}(2^n-1))$ for any integer $n \geqslant 1$.

Proof. The renormalization step of the free entanglement lattice shown in Fig. 7 is applied to $D_{\mathcal{F}}$ by using the triangle inequality on paired contributions to the cost function

$$\sum_{a=0,1} |\rho_{\pi(a,b)} - \sigma_{(a,b)}| \geqslant \left| \sum_{a=0,1} \rho_{\pi(a,b)} - \sum_{a=0,1} \sigma_{(a,b)} \right| \geqslant |\rho'_{\pi(b)} - \sigma'_{(b)}|, \tag{A3}$$

where π is a map from the occupation numbers of σ to the eigenvalue ordering of ρ. We denote with a the occupation number of a distinguished mode and b is a tuple carrying the occupancies of all the other modes. When the degeneracy is $N = 2^{n+1} - 2$, there is no ambiguity in the assignment of occupations to the spectrum of ρ because the final two levels are always the fully occupied pattern $(1,1,\dots)$ and the same but without a particle in the lowest-energy mode $(0,1,\dots)$. By integrating over the occupations of the lowest-energy mode in this way we produce a renormalized σ' and the renormalized flat spectrum ρ' which now has degeneracy $N' = 2^n - 1$. For the case of three fermionic modes, this is illustrated in Fig. 7 where the dashed ellipses group levels that are integrated together in this procedure. This provides a lower bound on $D_{\mathcal{F}}(\bar{\rho}(2^{n+1}-2))$ which is the same as the upper bound found by considering the direct sum ansatz $\frac{1}{2}(\sigma \oplus \sigma)$ demonstrating equality. ∎

Considering that from Ref. [8] we have an exact result $D_{\mathcal{F}}(\bar{\rho}_{(3)}) = 1/6$ we find as a corollary that $D_{\mathcal{F}}(\bar{\rho}_{(6)}) = D_{\mathcal{F}}(\bar{\rho}_{(3)}) = 1/6$ and hence the flat-spectrum upper bound is exact for $N = 6$. This is the largest N for which we have such a result aside from powers of 2.

We refer to this technique as entanglement lattice renormalization and it appears a promising direction for analytical methods to derive lower bounds to $D_{\mathcal{F}}$, something which is challenging since it is defined by a minimization problem. The difficulty in applying this method generally lies in dealing with all the different linear orderings compatible with the partial order. Theorem 1 falls in the special case where the ordering could be ignored, making it relatively simple.

4. Local equivalence between parafermion chain states

We have found that a $\mathbb{Z}_{pq}$ chain and $\mathbb{Z}_p \times \mathbb{Z}_q$ chain have equivalent entanglement and that this leads to $D_{\mathcal{F}} = 0$ for any eigenstate associated to any bipartition of a fixed-point $\mathbb{Z}_{2^n}$ chain. We may wonder how this equivalence for all cuts could be coherently extended to an equivalence between states. This can be achieved for the fixed-point parafermion chains as we will demonstrate. In particular, this means every eigenstate of a fixed-point $\mathbb{Z}_4$ chain is equivalent to a $\mathbb{Z}_2 \times \mathbb{Z}_2$ chain according to a local unitary.

This problem can be approached by first constructing a matrix product state (MPS) representation for the ground states of parafermion chains [44]. A translationally invariant MPS representation is a decomposition [45,46]

$$|\psi\rangle = \sum_{i_1,\dots,i_L} (\eta| \left(\prod_{j=1}^{L} \Gamma_{i_j} \right) |\rho) |i_1 i_2 \dots i_L\rangle \tag{A4}$$

into site tensor Γ and environment vectors $|\rho)$ and $(\eta|$. At the topological fixed point of a $\mathbb{Z}_N$ parafermion chain the site tensor can be chosen as

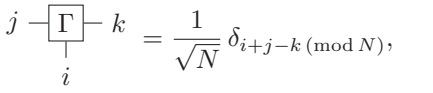

$$= \frac{1}{\sqrt{N}} \delta_{i+j-k \,(\mathrm{mod}\, N)}, \tag{A5}$$

where the basis indexed by i is the basis of eigenvectors of τ, with $\tau|i\rangle = \omega^i |i\rangle$. The bases indexed by j and k are contracted and summed over as the matrix product in (A4). The environment vectors can be chosen as $(\eta| = (0|$ and $|\rho) = |q)$ where q is the parafermionic parity of $|\psi\rangle$. It is simple to verify that the state (A4) is indeed normalized and also in the ground subspace of all the terms in the Hamiltonian.

We turn the equation which states the local transformation between the two states into an equation involving a gauge transformation A internal to the MPS, yielding

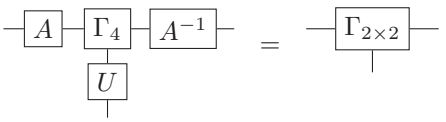

(A6)

where Γ_4 and $\Gamma_{2\times2} = \Gamma_2 \otimes \Gamma_2$ are site tensors for the $\mathbb{Z}_4$ and $\mathbb{Z}_2 \times \mathbb{Z}_2$ chains, respectively, and U is the local action of the unitary transformation between the states. This is a potentially difficult problem to solve in general, however, the states we consider are highly structured.

For each i we get a matrix slice of the site tensor Γ_i which transforms under the gauge transformations as $\Gamma_i \mapsto A\Gamma_i A^{-1}$. For the states we consider, we can use this gauge transformation in order to choose a basis in which every matrix slice of both Γ_4 and $\Gamma_{2\times2}$ is simultaneously diagonal. In this way, the site tensors can be interpreted as matrices, linear maps from the diagonal entanglement vector space spanned by $j = k$ to the physical vector space spanned by i. The equation for local-unitary equivalence of $\mathbb{Z}_4$ and $\mathbb{Z}_2 \times \mathbb{Z}_2$ parafermion chains then becomes

$$U \frac{1}{2} \begin{pmatrix} 1 & 1 & 1 & 1 \\ 1 & -i & -1 & i \\ 1 & -1 & 1 & -1 \\ 1 & i & -1 & -i \end{pmatrix} = \frac{1}{2} \begin{pmatrix} 1 & 1 & 1 & 1 \\ 1 & -1 & 1 & -1 \\ 1 & 1 & -1 & -1 \\ 1 & -1 & -1 & 1 \end{pmatrix}. \tag{A7}$$

This clearly has a solution for U as both matrices are unitary. The same method applies to relating $\mathbb{Z}_{pq}$ and $\mathbb{Z}_p \times \mathbb{Z}_q$ chains for any p and q.

We now turn to examine excited states. The τ operator creates a pair of excitations, a twist-antitwist pair

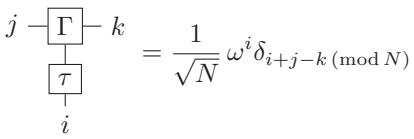

$$= \frac{1}{\sqrt{N}} \omega^i \delta_{i+j-k \,(\mathrm{mod}\, N)} \tag{A8}$$

which is diagonal in the same gauge as the unexcited site tensor. The effect of τ on the matrices of eigenvalues for $\mathbb{Z}_{pq}$ is to premultiply with a diagonal matrix $\mathrm{diag}(1,\omega,\omega^2,\dots)$. Considering the composite system $\mathbb{Z}_2 \times \mathbb{Z}_2$ chain we can create excitations on either of the two chains. The diagonal matrix thus formed features only 1 and -1 as opposed to the powers of $\omega = e^{2\pi i/4}$ found for the $\mathbb{Z}_4$ case. If we demand that Eq. (A7) is satisfied after inserting diagonal unitaries, it must be the case that the two diagonal matrices have the same eigenvalues. For the case of $\mathbb{Z}_4$ and $\mathbb{Z}_2 \times \mathbb{Z}_2$, this clearly is not possible as their eigenvalues are distinct. This is a special case of $\mathbb{Z}_p \times \mathbb{Z}_q$ for p and q with shared prime factors. In conclusion, a single unitary cannot be chosen in this case to map all the eigenstates of the $\mathbb{Z}_p \times \mathbb{Z}_q$ chain onto the $\mathbb{Z}_{pq}$ chain.

This is perhaps unsurprising because no symmetric finite depth unitary circuit can map between distinct symmetry-protected topological phases [47]. However, our situation is slightly different as the unitary we consider need not be symmetry preserving. Furthermore, its locality is particularly restricted as a tensor product of site-local unitaries. Even in this setting there does not exist a single unitary which transforms all the eigenstates of the $\mathbb{Z}_4$ chain to those of $\mathbb{Z}_2 \times \mathbb{Z}_2$ chain. Nevertheless, it is possible to find a different unitary in general for any single eigenstate. Similarly, for the string-net models it is clear that a unitary connecting $\mathbb{Z}_4$ and $\mathbb{Z}_2 \times \mathbb{Z}_2$ for all states cannot exist because these topologically ordered phases cannot be adiabatically connected [48], but this does not preclude the possibility of local unitaries for individual states.

5. Excited states of $\mathbb{Z}_4$ parafermions

We find that $D_{\mathcal{F}} = 0$ for the excited states of the $\mathbb{Z}_4$ parafermion chain at the fixed point $f = 0$. For some small finite $f > 0$, in the chiral phase $\phi = \frac{\pi}{2}$, $\theta = \pi$, $D_{\mathcal{F}}$ of the excited states of $\mathbb{Z}_4$ converges exponentially to zero. In general, however, for finite $f > 0$, excited states above single quasiparticle excitations have nonzero $D_{\mathcal{F}}$. This seems to suggest that the $\mathbb{Z}_4$ parafermion chain has free-fermion representations in certain parts of its phase diagram. In the recent work of Ref. [28], the authors present such a free-fermion representation for this model when the chirality angles are $\phi = \frac{n\pi}{2}$ and $\theta = m\pi$. They construct a canonical transformation mapping the $\mathbb{Z}_4$ parafermion chain to two decoupled $\mathbb{Z}_2$ chains at these angles. In Fig. 8 (top) we confirm these findings, showing that $D_{\mathcal{F}}$ converges exponentially to zero as we increase system size at $f = 0.1, \phi = \frac{\pi}{2}, \theta = \pi$. While in Fig. 8 (bottom) we show that at some arbitrary angles $\phi = \theta = 0.4$ ($f = 0.1$) $D_{\mathcal{F}}$ does converge for very low excited states but not for higher ones.

6. Distribution functions for Abelian string nets

Let the degeneracy of the flat entanglement spectrum be $\chi = N^k$ where N is the order of the associated Abelian group

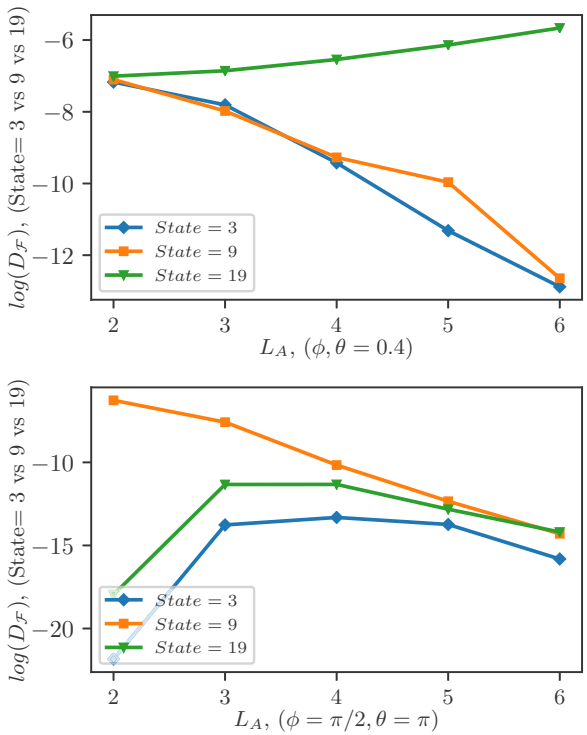

FIG. 8. (Top) The interaction distance for the $\mathbb{Z}_4$ chain's low-lying excited states at $f = 0.1$, $\phi = \theta = 0.4$. We see the two lower excited states (3rd and 6th) converge to zero as partition length is increased, but the 19th clearly does not. (Bottom) The interaction distance for the $\mathbb{Z}_4$ chain's low-lying excited states at $f = 0.1$, $\phi = \frac{\pi}{2}$, $\theta = \pi$. All states converge to zero as the partition length is increased.

and $k = |\partial A| - b_0$ is the number of independent degrees of freedom on the b_0-component boundary ∂A. We seek the distribution $P(D_{\mathcal{F}})$ for these spectra obtained by varying either N or k. As an intermediate step, we will find the density function for $P(a)$ or equivalently $P(\alpha)$, where $a = \log_2 \chi \pmod 1$ and $\alpha = 2^a$ are variables describing the position of χ between powers of 2.

Consider first evaluating $D_{\mathcal{F}}$ for varying $k \in \mathbb{N}$, i.e., the subsystem size, while keeping N fixed. If $\log_2 N$ is irrational, then $a = k \log_2 N \pmod 1$ for each k, which uniformly samples the interval $[0,1]$ and hence $P(a) = 1$ over that interval. In Fig. 9 we compare this prediction for fixed N against the sample of k up to $2^{15} - 1$.

If we instead fix $k = 1$ and vary $N \in \mathbb{N}$, while mapping each interval between powers of 2 back onto the interval $\alpha \in [1,2]$, we find that it is densely and uniformly sampled in the limit of the infinite sequence, giving $P(\alpha) = 1$. The case $k = 1$ refers to a rather unphysical subsystem containing zero vertices and one edge going through the cut, which is however equivalent to cutting a single interval of lattice sites from the parafermion chain.

The situation is more complicated for $k > 1$. For instance, when $k = 2$, region A corresponds to a disk enclosing a single trivalent vertex. These sequences of spectra are also found in the parafermion chain when region A comprises k disjoint intervals. We first collapse all the natural numbers into the interval $[1,x]$ where $x = 2^{1/k}$ in the same manner

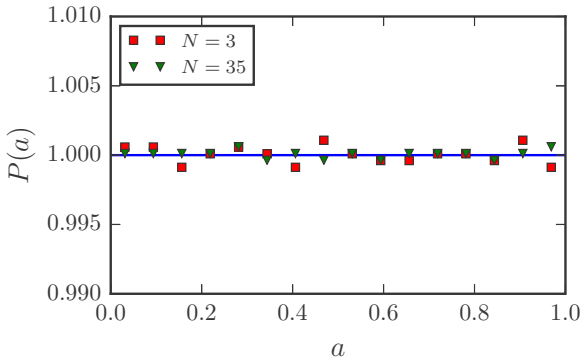

FIG. 9. Distribution $P(a)$ for varying k in the cases of $N = 3$ and 35. The line is the analytic result $P(a) = 1$. The markers are numerical results for a sample up to $k = 2^{15} - 1$.

as for $k = 1$ to find $P(\beta) = 1/(x - 1)$, where β identifies a corresponding real number for that integer in the interval. Notice that $a = \log_x \beta$ and thus

$$P(a) = P(\beta)\frac{d\beta}{da} = \frac{\ln 2}{k(2^{1/k} - 1)}2^{a/k}. \tag{A9}$$

In Fig. 10 we show the validity of our prediction for fixed k for sample obtained by varying N up to 2^{18}.

Armed with the distributions $P(a)$ or $P(\alpha)$ for the processes under discussion, we can straightforwardly calculate the corresponding distributions for $D_{\mathcal{F}}$ for fixed N,

$$P(D_{\mathcal{F}}) = \frac{2/\ln 2}{\sqrt{1 + D_{\mathcal{F}}(D_{\mathcal{F}} - 6)}}, \tag{A10}$$

which was presented in the main text, and for fixed large k which is

$$P(D_{\mathcal{F}}) = \frac{3 - D_{\mathcal{F}}}{\sqrt{1 + D_{\mathcal{F}}(D_{\mathcal{F}} - 6)}}. \tag{A11}$$

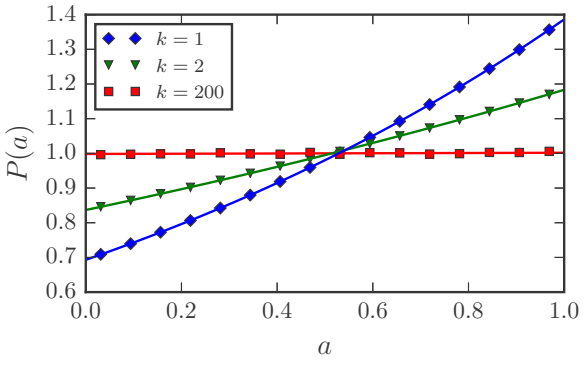

FIG. 10. Distribution $P(a)$ obtained by varying n for $k = 1$, 2, and 200. The curves are the analytic result of (A9). The markers are numerical results for a sample up to $N = 2^{18}$. Statistical errors are too small to be visible. We see that as k is increased, $P(a)$ approaches the uniform distribution as expected.

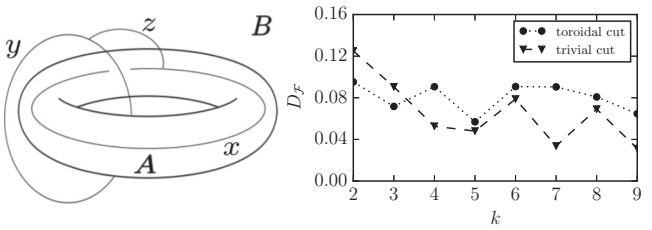

FIG. 11. Shows a topologically nontrivial toroidal cut of a Walker-Wang model (left). A plot of $D_{\mathcal{F}}$ against k level for a toroidal and a topologically trivial partition, both with $|\partial A| = 3$ (right).

Expanding the formula for fixed k in a Taylor series for small $1/k$ we find

$$P(a) = 1 + \left(a - \frac{1}{2}\right)\frac{\ln 2}{k} + \frac{\left(a - \frac{1}{2}\right)^2 - \frac{1}{12}}{2}\left(\frac{\ln 2}{k}\right)^2 + O\left(\frac{1}{k^3}\right), \tag{A12}$$

and hence

$$P(a) + P(1 - a) = 1 + O\left(\frac{1}{k^2}\right). \tag{A13}$$

This implies that corrections to the large-k form of $P(D_{\mathcal{F}})$ are of order $1/k^2$ because $P(D_{\mathcal{F}})$ is proportional to $P(a) + P(1 - a)$ for a such that $D_{\mathcal{F}}(\bar{\rho}(2^a)) = D_{\mathcal{F}}$. These are the only two values of a to produce the same $D_{\mathcal{F}}$ and $D_{\mathcal{F}}$ viewed as a function of a is invariant under the transformation $a \mapsto 1 - a$.

Walker-Wang models. While the string-net models can be directly generalized to three spatial dimensions, a more powerful generalization has been recently given in terms of the Walker-Wang models [11]. These models allow nontrivial braiding of the charges giving a rich behavior in their bulk and at their boundary [49,50].

The entanglement spectrum for topologically trivial cuts of a Walker-Wang model can be found in the same way as for string nets given by $\rho_a = (\prod_{j\in a} d_{x_j})/\mathcal{D}^{2(|\partial A|-1)}$ in the main text. Nevertheless, partitions with nontrivial boundary topology reveal novel correlation properties [33]. To identify their effect on the interaction distance, we take the region A with a boundary topologically equivalent to a torus, as shown in Fig. 11 (left). Among the allowed configurations in the ground state is a braiding of loops with charges x and y supported in A and B, respectively, connected by a string of charge z piercing ∂A [33]. Thus, the probability spectrum should now encode information about the nontrivial braiding of the charges. In Fig. 11 (right) we show $D_{\mathcal{F}}$ for toroidal cuts of non-Abelian $\mathrm{SU}(2)_k$ Walker-Wang models as a function of the level $k \geqslant 2$. Compared to the spherical cut we see that the interaction distance depends not only on the geometry of the cut, but also on the topology of ∂A. Its nonzero value indicates the necessity of interactions for the existence of non-Abelian topological order also in three dimensions.

[1] X. G. Wen, Int. J. Mod. Phys. B **04**, 239 (1990).
[2] J. M. Leinaas and J. Myrheim, Il Nuovo Cimento B (1971-1996) **37**, 1 (1977).
[3] F. Wilczek, Phys. Rev. Lett. **49**, 957 (1982).
[4] P. W. Anderson, Science **235**, 1196 (1987).
[5] D. C. Tsui, H. L. Stormer, and A. C. Gossard, Phys. Rev. Lett. **48**, 1559 (1982).
[6] N. Read and D. Green, Phys. Rev. B **61**, 10267 (2000).
[7] D. A. Ivanov, Phys. Rev. Lett. **86**, 268 (2001).
[8] C. J. Turner, K. Meichanetzidis, Z. Papic, and J. K. Pachos, Nat. Commun. **8**, 14926 (2017).
[9] P. Fendley, J. Stat. Mech.: Theor. Exp. (2012) P11020.
[10] M. A. Levin and X.-G. Wen, Phys. Rev. B **71**, 045110 (2005).
[11] K. Walker and Z. Wang, Front. Phys. **7**, 150 (2012).
[12] A. Kitaev, Ann. Phys. **321**, 2 (2006), Special Issue.
[13] H. Li and F. D. M. Haldane, Phys. Rev. Lett. **101**, 010504 (2008).
[14] I. Peschel and V. Eisler, J. Phys. A: Math. Theor. **42**, 504003 (2009).
[15] T. D. Schultz, D. C. Mattis, and E. H. Liev, Rev. Mod. Phys. **36**, 856 (1964).
[16] A. Y. Kitaev, Phys. Usp. **44**, 131 (2001).
[17] E. Fradkin and L. P. Kadanoff, Nucl. Phys. B **170**, 1 (1980).
[18] J. Alicea and P. Fendley, Annu. Rev. Condens. Matter Phys. **7**, 119 (2016).
[19] D. J. Clarke, J. Alicea and K. Shtengel, Nat. Phys. **10**, 877 (2014).
[20] R. S. K. Mong, D. J. Clarke, J. Alicea, N. H. Lindner, P. Fendley, C. Nayak, Y. Oreg, A. Stern, E. Berg, K. Shtengel, and M. P. A. Fisher, Phys. Rev. X **4**, 011036 (2014).
[21] J. Motruk, E. Berg, A. M. Turner, and F. Pollmann, Phys. Rev. B **88**, 085115 (2013).
[22] W. Li, S. Yang, H.-H. Tu, and M. Cheng, Phys. Rev. B **91**, 115133 (2015).
[23] S. Elitzur, R. B. Pearson, and J. Shigemitsu, Phys. Rev. D **19**, 3698 (1979).
[24] T. J. Osborne and F. Verstraete, Phys. Rev. Lett. **96**, 220503 (2006).
[25] K. Meichanetzidis, J. Eisert, M. Cirio, V. Lahtinen, and J. K. Pachos, Phys. Rev. Lett. **116**, 130501 (2016).
[26] S. R. White, Phys. Rev. Lett. **69**, 2863 (1992).
[27] U. Schollwöck, Ann. Phys. **326**, 96 (2011).
[28] N. Moran, D. Pellegrino, J. K. Slingerland, and G. Kells, Phys. Rev. B **95**, 235127 (2017).
[29] M. A. Nielsen and I. L. Chuang, *Quantum Computation and Quantum Information: 10th Anniversary Edition*, 10th ed. (Cambridge University Press, New York, 2011).
[30] P. W. Shor, SIAM J. Comput. **26**, 1484 (1997).
[31] R. Cleve, A note on computing Fourier transforms by quantum programs, 1994 (unpublished).
[32] C.-H. Lin and M. Levin, Phys. Rev. B **89**, 195130 (2014).
[33] A. Bullivant and J. K. Pachos, Phys. Rev. B **93**, 125111 (2016).
[34] A. Kitaev, Ann. Phys. **303**, 2 (2003).
[35] H. Yao and X.-L. Qi, Phys. Rev. Lett. **105**, 080501 (2010).
[36] S. Trebst, M. Troyer, Z. Wang, and A. W. W. Ludwig, Prog. Theor. Phys. Suppl. **176**, 384 (2008).
[37] J. K. Pachos, *Introduction to Topological Quantum Computation* (Cambridge University Press, Cambridge, 2012).
[38] B. Sutherland, *Beautiful Models: 70 Years of Exactly Solved Quantum Many-body Problems* (World Scientific, Singapore, 2004).
[39] V. Lahtinen and J. K. Pachos, New J. Phys. **11**, 093027 (2009).
[40] B. A. Davey and H. A. Priestley, *Introduction to Lattices and Order*, Cambridge Mathematical Textbooks (Cambridge University Press, Cambridge, 2002).
[41] T. Brylawski, Discrete Math. **6**, 201 (1973).
[42] M. A. Nielsen, Phys. Rev. Lett. **83**, 436 (1999).
[43] G. Vidal, D. Jonathan, and M. A. Nielsen, Phys. Rev. A **62**, 012304 (2000).
[44] W.-T. Xu and G.-M. Zhang, Phys. Rev. B **95**, 195122 (2017).
[45] M. Fannes, B. Nachtergaele, and R. F. Werner, Commun. Math. Phys. **144**, 443 (1992).
[46] R. Orus, Ann. Phys. **349**, 117 (2014).
[47] X. Chen, Z.-C. Gu, Z.-X. Liu, and X.-G. Wen, Phys. Rev. B **87**, 155114 (2013).
[48] X. Chen, Z.-C. Gu, and X.-G. Wen, Phys. Rev. B **82**, 155138 (2010).
[49] C. W. von Keyserlingk, F. J. Burnell, and S. H. Simon, Phys. Rev. B **87**, 045107 (2013).
[50] C. W. von Keyserlingk and F. J. Burnell, Phys. Rev. B **91**, 045134 (2015).